Biophysical Journal Volume 80 March 2001 1115–1123

Protein Flexibility from the Dynamical Transition: A Force Constant Analysis

D. J. Bicout*† and G. Zaccai†‡

*INFM-Operative Group Grenoble CRG IN13 and †Institut Laue-Langevin, 38042 Grenoble Cedex 9, France; and ‡Laboratoire de Biophysique Moléculaire, Institut de Biologie Structurale, F-38027 Grenoble Cedex 1, France

ABSTRACT A standard analysis of the scattered neutron incoherent elastic intensity measured with very good energy resolution yields elastic scans, i.e., mean-square displacements of atomic motions (in a pico to nanosecond time scale) in a sample as a function of temperature. This provides a quick way for characterizing the dynamical behavior of biological macromolecules, such behavior being correlated with biological function and activity. Elastic scans of proteins exhibit a dynamical transition at ~200 K, marking a cross-over in molecular fluctuations between harmonic and nonharmonic dynamical regimes. This paper presents an approach allowing analysis of the elastic scan in terms of force constants and related parameters, such as the free energy barrier ΔG at the transition. We find that the increased protein flexibility beyond the dynamical transition is associated with $\Delta G \sim RT$ and effective force constants of the order of 0.1–3 N/m. The analysis provides a set of parameters for characterizing molecular resilience and exploring relations among dynamics, function, and activity in proteins.

INTRODUCTION

Molecular dynamics plays an important role in enzyme catalysis and other aspects of biological activity, such as receptor-ligand binding or proton or ion pumping in membrane proteins. The motions involved cover several orders of magnitude in time from the femtosecond for electronic rearrangements, via the picosecond to nanosecond for thermal fluctuations, the millisecond of conformational changes involved in functional kinematics, to the seconds and minutes of protein kinesis and cell division. In the present study we are concerned with thermal molecular motions reflecting the forces that maintain biological tertiary and quaternary structure. They arise from H-bonding, electrostatic and van der Waals interactions, and pseudo-forces associated with the hydrophobic effect (Creighton, 1991). Their associated energies are of the order of a few kcal/mol and atomic thermal fluctuations are of the order of 1 Å.

To characterize dynamics-function and dynamics-activity relationships in molecular and cell biology, it is necessary to study the molecular flexibility of as many different protein systems in as many different conditions as possible. It has been observed that proteins undergo a dynamical transition as a function of temperature that marks the cross-over in molecular fluctuations between the harmonic behavior dominated by vibrational motions at low temperatures and a nonharmonic dynamical regime involving barrier crossing processes at higher temperatures (Parak et al., 1982; Doster et al., 1989). Protein molecular fluctuations are of low and high amplitude below and above the transition, respectively. Similarly, protein flexibility and the ability to undergo conformational changes appear to be low below and increase above the transition. It has been found that protein activity is inhibited when the temperature is lowered below the transition (Rasmussen et al., 1992; Ferrand et al., 1993; Lehnert et al., 1998). Thus, to characterize the relation among protein dynamics, function, and activity it is important to achieve a good understanding of the dynamical transition. The role played by the solvent in the dynamical transition has been examined recently (Réat et al., 2000).

Neutron scattering is particularly suited to the study of thermal molecular motions because neutrons of 1 Å wavelength have an energy close to 1 kcal/mol. Thermal motions have been shown to be correlated with the ability of a protein to undergo functional conformational changes (Lehnert et al., 1998), and they can be seen as the lubricant that makes possible such displacements taking place on a much longer time scale (Brooks III et al., 1988). Depending on the energy resolution of the spectrometer, neutron scattering can be used to observe 1) elastic scattering, from which mean-square fluctuations in a given time scale can be calculated (Doster et al., 1989); 2) quasielastic scattering, from which correlation times of diffusion motions can be calculated (Bée, 1988; Fitter et al., 1996); and 3) inelastic scattering, arising from vibrational modes (e.g., Cordone et al., 1999).

The elastic experiments are the most efficient to perform, having the best signal-to-noise ratio. On backscattering spectrometers a time scale up to ~0.1 ns can be achieved (matching well with thermal motions) and a standard analysis as a function of scattering vector Q yields values for the mean-square displacements, dominated by H (hydrogen) atom motions in the sample because their incoherent cross section is an order of magnitude larger than that of other atoms (Smith, 1991). In the time scale examined, however, H atoms reflect the global thermal behavior of a sample because they move with the larger chemical groups, such as

Received for publication 9 June 2000 and in final form 13 December 2000.

Address reprint requests to D. J. Bicout, Institut Laue-Langevin, 6 Rue Jules Horowitz, B.P. 156, 38042 Grenoble Cedex 9, France. Tel.: 33-4-76-207228; Fax: 34-4-76-882416; E-mail: bicout@ill.fr.

0006-3495/01/03/1115/09 $2.00

amino acid side chains, to which they are bound (Smith, 1991; Réat et al., 1998).

An elastic scan (i.e., the plot of the molecular mean-square displacements as a function of absolute temperature) of myoglobin revealed the dynamical transition at ~180 K (Parak et al., 1982; Doster et al., 1989). Doster et al. analyzed the dynamical transition in terms of a double-well potential model for the side-chain motions in the protein and calculated the displacement and free energy difference between the two wells. Related to this is the conformational substate model developed by Frauenfelder and collaborators (Frauenfelder et al., 1988) in which the protein atoms are trapped in harmonic potential wells at low temperature and can sample different wells when the activation energy becomes available above the transition temperature. Other models, such as diffusion motions in cages (Kneller and Smith, 1994) and molecular dynamics simulations (Loncharich and Brooks, 1990; Smith et al., 1990) have also been used to analyze the dynamical transition. Since the myoglobin experiments, the dynamical transition has been observed in other soluble proteins (Andreani et al., 1995) and membranes (Ferrand et al., 1993).

Experimentally, each point on an elastic scan provides a value for the molecular mean-square displacement at the temperature under consideration. Below the transition temperature, i.e., in the harmonic regime, the slope (i.e., the derivative of the mean-square displacement with respect to the temperature) of the elastic scan has the dimension of k_B/k, where k_B is the Boltzmann constant and the "force constant" k has the dimension of force per unit length. In the vicinity and above the transition temperature, i.e., in the nonharmonic regime, the direct use of this definition leads to a temperature-dependent force constant that simply indicates that additional parameters are involved. In this paper we develop a simple model in which the mean-square displacement shows the dynamical transition as a function of temperature. We derive an expression for the mean-square displacement versus temperature, valid for all dynamical regimes from harmonic to nonharmonic. This analysis approach allows us to determine the transition temperature, the force constants, and relevant parameters of the problem. These quantities are used to characterize the molecular resilience of a macromolecule and to compare different systems (Zaccai, 2000a) in the exploration of relations between dynamics with biological function and activity.

THEORETICAL BACKGROUND

Let us consider the incoherent scattering of neutrons by hydrogen nuclei in a protein. These particles undergo motions in the potential $V(\mathbf{r})$, where $\mathbf{r}(t)$ denotes the position vector of the particle at time t. The function of interest describing the scattering process is the incoherent intermediate scattering function $I(\mathbf{Q}, t)$ given by

$$I(\mathbf{Q}, t) = \sum_{\alpha=1}^{N} x_\alpha \langle e^{i\mathbf{Q}\cdot\mathbf{r}_\alpha(t)} e^{-i\mathbf{Q}\cdot\mathbf{r}_\alpha(0)} \rangle, \quad (1)$$

where $x_\alpha (\Sigma_{\alpha=1}^{N} x_\alpha = 1)$ is the fraction of particles experiencing the same dynamics in the potential $V_\alpha(\mathbf{r})$, $\mathbf{Q}$ is the scattering wavevector of the neutrons, and brackets denote the ensemble average over many trajectories for a population of particles initially at thermal equilibrium. For small $\mathbf{Q}$ (i.e., in the Gaussian scattering approximation) one can perform the orientational average to eliminate angular coordinates yielding

$$I(Q, t) \cong \sum_{\alpha=1}^{N} x_\alpha \exp\left\{ -\frac{Q^2}{6} \langle [\mathbf{r}_\alpha(t) - \mathbf{r}_\alpha(0)]^2 \rangle \right\}. \quad (2)$$

Note that because of the polydispersity in particle dynamics (i.e., $x_\alpha \neq 1$), the intensity in Eq. 2 results from a combination of several Gaussian functions, and thus is no longer Gaussian as a function of Q (Smith et al., 1990). The mean-square displacement in this expression can be written as $\langle [\mathbf{r}_\alpha(t) - \mathbf{r}_\alpha(0)]^2 \rangle = 2\langle r_\alpha^2 \rangle [1 - C_\alpha(t)]$, where $\langle r_\alpha^2 \rangle$ is the equilibrium mean-square displacement and $C_\alpha(t)$ the stationary position relaxation function (determination of which requires to know the self-pair correlation function describing the time propagation of the particle in the potential). Clearly, the mean-square displacement in Eq. 2 reduces to the equilibrium value $2\langle r_\alpha^2 \rangle$ for times long enough such that $C_\alpha(t) \to 0$.

The function measured in incoherent neutron scattering experiments is the incoherent dynamic structure factor $S_{inc}(Q, \omega)$, where $\hbar\omega$ is the energy transfer from the neutron beam to the system. This function is the Fourier transform of $I(Q, t)$ and consists of the summation of two components: an "elastic" component $S_{inc}^{el}(Q) = S_{inc}(Q, \omega = 0) = I(Q, \infty)\delta(\omega)$ plus a quasielastic component that involves energies $\omega > 0$. In what follows we focus only on the elastic component because we are interested in studying the spatial distribution of particle motions. However, if τ is the resolution time of the experiment, $S_{inc}^{el}(Q)$ is related to the normalized elastic intensity by

$$S_{inc}^{el}(Q) \simeq I(Q, \tau) = \sum_{\alpha=1}^{N} x_\alpha \exp\left\{ -\frac{Q^2 \langle r_\alpha^2 \rangle}{3} [1 - C_\alpha(\tau)] \right\}. \quad (3)$$

Thus, because of finite resolution time $S_{inc}^{el}(Q)$ includes both $\langle r_\alpha^2 \rangle$ and $C_\alpha(\tau)$. It eventually relaxes to $I(Q, \infty)$, which depends only on $\langle r_\alpha^2 \rangle$ when the resolution time is long enough such that all $C_\alpha(\tau) \to 0$. The observed mean-square displacement, $\langle R^2 \rangle$, which takes into account fluctuations of all

particles in the protein system, is given by:

$$\langle R^2\rangle = -3\left.\frac{d\{\ln[S^{el}_{inc}(Q)]\}}{d(Q^2)}\right|_{Q=0}$$

$$= \sum_{\alpha=1}^{N} x_\alpha\langle r_\alpha^2\rangle[1 - C_\alpha(\tau)]. \quad (4)$$

Nonetheless, for a given experiment $C_\alpha(\tau)$ is a constant that rescales the observed mean-square displacement. Thus, without loss of generality, we can assume from now on that $C_\alpha(\tau) = 0$ for particles under study.

FORMULATION OF THE MODEL ANALYSIS

For the sake of simplicity we introduce the model by assuming that all particles are dynamically equivalent, i.e., $x_\alpha = 1$. In the spirit of mode coupling theory (Götze and Sjögren, 1992), the model assumes that two classes of conformational fluctuations essentially control atomic motions in a protein in the native state. First are fluctuations of the local environment in which the particle undergoes movements about its equilibrium position. Second are interaction-mediated fluctuations of the protein molecule that allow larger excursions of the particle within a cage formed by its neighboring molecules. For a protein atom this can be regarded as two, i.e., a large and a small, conformational cages fitting together within which it is compelled to move in a potential $V(\mathbf{r})$. Many conformational substates for the protein in the native state may correspond to the same position $\mathbf{r}$ of the particle at time t.

Specifically, we consider in each conformational cage the vibrational and translational motions of the particle (other degrees of freedom, such as rotation, are ignored for simplicity). As customary, we assume that $\mathbf{r}(t)$ can be split into two independent components, $\mathbf{r}(t) = \mathbf{r}_v(t) + \mathbf{r}_t(t)$, where the vibrational component $\mathbf{r}_v(t)$ is the displacement about the equilibrium position within the host molecule and the translational part $\mathbf{r}_t(t)$ is the instantaneous location of the equilibrium position at time t. For a spherically symmetric potential, $V(r)$ is given by:

$$V(r) = V(r_v, r_t) = \tfrac{1}{2}k_v(r_t)r_v^2 + U(r_t), \quad (5)$$

where $k_v(r_t)$ is the vibrational force constant that depends on the equilibrium position of the particle. The potential $U(r_t)$ for translational motions has a double-well structure with a barrier at $r_t = r_t^\#$ such that $U(r_t^\#) > k_BT$, where $\beta^{-1} = k_BT$ is the thermal energy. We have $k_v(r_t) = k_{vs}$ for $0 \le r_t \le r_t^\#$ (small conformational cage) and $k_v(r_t) = k_{vl}$ for $r_t > r_t^\#$ (large conformational cage); that is to say that the particle vibrational motions are harmonic in both small and large conformational cages, but with different frequencies. Protein conformations corresponding to particle positions such that $r_t \le r_t^\#$ are energetically more stable than those corresponding to $r_t > r_t^\#$ because larger excursions of the particle require a displacement of several neighboring molecules.

In this model, the coordinates $\mathbf{r}_v(t)$ and $\mathbf{r}_t(t)$ describe the harmonic vibration and nonharmonic translation motions, respectively. We now use this potential to calculate the normalized elastic intensity.

Elastic incoherent structure factor

The elastic incoherent structure factor, $I(Q, \infty)$, for the potential in Eq. 5 is given by:

$$I(Q,\infty) = \left|\frac{\int e^{i\mathbf{Q}\cdot\mathbf{r}}e^{-\beta V(\mathbf{r})}d\mathbf{r}}{\int e^{-\beta V\mathbf{r}}d\mathbf{r}}\right|^2$$

$$= |(1-\phi)e^{-Q^2\langle r_{vs}^2\rangle/6}F_s(Q) + \phi e^{-Q^2\langle r_{vl}^2\rangle/6}F_l(Q)|^2, \quad (6)$$

where the exponentials in Eq. 6 represent the Debye-Waller factors in each cage with $\langle r_{vs}^2\rangle$ and $\langle r_{vl}^2\rangle$ being the vibrational mean-square displacement of the particle in small and large cages, respectively. The scattering amplitudes $F_s(Q)$ and $F_l(Q)$ for translation motions in small and large cages, respectively, are given in the Gaussian approximation by:

$$F_s(Q) = \frac{1}{Z_{ts}}\int_0^{r\#} dr_t r_t^2 e^{-\beta U(r_t)}\left[\frac{\sin(Qr_t)}{Qr_t}\right] \simeq e^{-Q^2\langle r_{ts}^2\rangle/6} \quad (7a)$$

$$F_l(Q) = \frac{1}{Z_{tl}}\int_{r\#}^{\infty} dr_t r_t^2 e^{-\beta U(r_t)}\left[\frac{\sin(Qr_t)}{Qr_t}\right] \simeq e^{-Q^2\langle r_{tl}^2/6}, \quad (7b)$$

where $\langle r_{ts}^2\rangle$ and $\langle r_{tl}^2\rangle$ are the mean-square displacement for translational motions of the particle in small and large conformational cages, respectively. The probability ϕ, which is the fraction of equivalent particles probing only the large conformational cage, is given by:

$$\phi = \frac{1}{1 + e^{\beta\Delta G}};$$
$$\Delta G = k_BT\ln\left[\frac{Z_{vs}Z_{ts}}{Z_{vl}Z_{tl}}\right] = \Delta H - T\Delta S, \quad (8)$$

where Z_{vs} and Z_{vl}, and Z_{ts} and Z_{tl} are the partition functions for vibration and translation coordinates, respectively. The ΔH and ΔG are the energy and free energy differences for the system in the large and small cages, and ΔS is the total conformational entropy difference between the two cages. The ratio $\phi/(1 - \phi) = e^{-\beta\Delta G}$ gives to some extent the frequency ratio of the large-to-small amplitude fluctuations of the protein molecule. Protein fluctuations are mostly of small amplitude when $\phi \sim 0$ at low temperature, while they are of larger amplitude for $\phi \sim 1$ when the temperature gets higher. Accordingly, one can define a temperature T_m at which small and large fluctuations occur with equal fre-

quency, i.e., when $\Delta G(T_m) = 0$ resulting from the compensation of the energy and entropy difference. Assuming that ΔH is independent of temperature, we have $T_m = \Delta H/\Delta S$.

Mean-square displacement

Placing the expression in Eq. 6 into Eq. 4 with $C_\alpha(\tau) = 0$, the mean-square displacement, $\langle R^2 \rangle$, of the particle is readily obtained as:

$$\langle R^2 \rangle = (1 - \phi)[\langle r_{vs}^2 \rangle + \langle r_{ts}^2 \rangle] + \phi[\langle r_{vl}^2 \rangle + \langle r_{tl}^2 \rangle]$$
$$= (1 - \phi)\langle r_s^2 \rangle + \phi \langle r_l^2 \rangle. \quad (9)$$

Although $\mathbf{r}_v$ and $\mathbf{r}_t$ are supposed to be independent, this expression clearly shows that the splitting $\langle r^2 \rangle = \langle r_v^2 \rangle + \langle r_t^2 \rangle$ makes sense only within each conformational cage, but not for the total mean-square displacement. Therefore, it is more convenient to define $\langle r_s^2 \rangle$ and $\langle r_l^2 \rangle$ as the overall mean-square displacement of the particle moving within the small and large conformational cages.

For a set of quantized harmonic oscillators the mean-square displacement is given by $\langle r^2 \rangle = k_B\theta/2k \tanh(\theta/2T)$, where $\theta = \hbar\omega_0/k_B$ is the Debye temperature and ω_0 and k are the frequency and force constant of the oscillator, respectively. For $T < \theta/2$ the mean-square displacement is almost a constant equal to the zero-point fluctuations $k_B\theta/k$, while it linearly increases with the temperature for $T > \theta/2$. Thus, the mean-square displacements in Eq. 9 originating from harmonic vibrational motions can be written as,

$$\langle r_{vs}^2 \rangle = \frac{k_B\theta}{2k_{vs}} \operatorname{cotanh}\left[\frac{\theta}{2T}\right]; \quad \langle r_{vl}^2 \rangle = \frac{k_BT}{k_{vl}}, \quad (10)$$

where the classical limit is taken for $\langle r_{vl}^2 \rangle$ since it contributes only at high T.

For the translational motions, however, the cages to the particle motions originate from the neighboring molecules that move due to structural fluctuations, as in the liquid state. This is represented by the potential $U(r_t)$, which has a double-well structure. In order to introduce the force constants, we invoke the linear approximation for the particle motion about each bottom well of $U(r_t)$, the translation mean-square displacement of the particle within each well of $U(r_t)$ can be written as,

$$\langle r_{ts}^2 \rangle = \frac{k_BT}{k_{ts}}; \quad \langle r_{tl}^2 \rangle = \frac{k_BT}{k_{tl}}, \quad (11)$$

where k_{ts} and k_{tl} can be regarded as equivalent force constants for translational motion in small and large conformational cages, respectively.

Equations 10 and 11 taken together into Eq. 9 can be recast in the formula,

$$\langle R^2(T) \rangle = [1 - \phi(T)]\left[\frac{k_B\theta}{2k_{vs}} \operatorname{cotanh}\left(\frac{\theta}{2T}\right) + \frac{k_BT}{k_{ts}}\right]$$
$$+ \phi(T)\left[\frac{k_BT}{k_{vl}} + \frac{k_BT}{k_{tl}}\right], \quad (12a)$$

which, when neglecting quantum effects for $T > \theta/2$, simplifies to:

$$\langle R^2(T) \rangle = [1 - \phi(T)]\frac{k_BT}{k_1} + \phi(T)\frac{k_BT}{k_2};$$
$$\begin{cases} k_1^{-1} = k_{vs}^{-1} + k_{ts}^{-1}, \\ k_2^{-1} = k_{vl}^{-1} + k_{tl}^{-1}, \end{cases} \quad (12b)$$

where k_1 and k_2 are the resulting force constants (from both the vibration and translation) to particle motions in small and large conformational cages. As a consequence of invoking the linear approximation for translational motions, vibrational and translational motions are merged into a single force constant k_i ($i = 1, 2$) in respective cages. Relaxing (or the failure of) the linear approximation would lead to nonlinear dependence of $\langle r_i^2 \rangle$ as a function of T (i.e., nonharmonic and temperature-dependent force constant), and thus to a distinction between the two types of motions. The nonharmonic behavior of $\langle R^2(T) \rangle$ in Eq. 12b arises because of finite fraction $\phi(T)$ describing the relative contribution of population of particles probing the large conformational cage. We will see further that the dynamical transition, defined as the deviation from the linear behavior of $\langle R^2(T) \rangle$ versus T, takes place for a value of ϕ that is rather small, i.e., when a small fraction of the total population of particles experience barrier crossing events caused by large amplitude fluctuations of the protein conformations. Equation 12b also suggests that within the linear (merging) approximation the harmonic regime at low temperature may involved degrees of freedom other than vibration because the translational force constant also contributes to k_1.

The generalization of Eq. 12b to dynamically nonequivalent particles is straightforwardly obtained as,

$$\langle R^2(T) \rangle = \sum_{\alpha=1}^{N} x_\alpha \left\{[1 - \phi_\alpha(T)]\frac{k_BT}{k_{1\alpha}} + \phi_\alpha(T)\frac{k_BT}{k_{2\alpha}}\right\}. \quad (13)$$

This expression can again be rewritten in the same form as Eq. 12b where now $\phi = \Sigma_{\alpha=1}^{N} x_\alpha\phi_\alpha$, and k_1 and k_2 will be the effective force constants which are functions of x_α, ϕ_α, and $k_{1\alpha}$ and $k_{2\alpha}$, respectively, and thus functions of temperature. However, it is plausible to consider, and we will do so from now on, that k_1 and k_2 are almost independent of T within the range of temperatures under consideration, and that the overall temperature dependence of the problem is entirely contained in the fraction $\phi(T)$, which is still given

by Eq. 8. In this respect, ΔG in Eq. 8 represents the mean free energy difference, i.e., $\Delta G = \Sigma_{\alpha=1}^{N} x_\alpha \Delta G_\alpha$, and k_1 and k_2 in Eq. 12b are the expected force constants associated with the small and large conformational cages, respectively.

Finally, it may be instructive in closing this subsection to mention the difference between Eqs. 12a and 12b and the expression used by Doster et al., 1989, which writes in our notation $\langle R^2(T)\rangle = \langle r_v^2\rangle + \phi(1-\phi)\langle r_t^2\rangle$. This relation is obtained for the jump model between the two minima (points) separated by a constant (T-independent) distance $\sqrt{\langle r_t^2\rangle}$ of a double well and assuming identical vibrational motions (i.e., $\langle r_v^2\rangle$) in the two wells. In contrast, our description considers the entire well (cages, not points), allows different $\langle r_v^2\rangle$ in each well, and treats the inter-well translational transition as a continuous process. If it is assumed in Eq. 9 that $\langle r_{vs}^2\rangle = \langle r_{vs}^2\rangle = \langle r_v^2\rangle$, Eq. 12b becomes $\langle R^2(T)\rangle = \langle r_v^2\rangle + (1-\phi)\langle r_{ts}^2\rangle + \phi\langle r_{tl}^2\rangle$, indicating and underlining that the nonharmonic behavior of $\langle R^2(T)\rangle$ originates from barrier crossing events in the translational motions.

Transition temperature

From what precedes and according to Eq. 12b, the mean-square displacement linearly increases with T with a slope k_B/k_1 at low temperature ($\phi \sim 0$). In practice, one is interested to locate the temperature about which the departure from the straight line of slope k_B/k_1 is effective and then determine the temperature for the dynamical transition. To this end, since the transition from low to high temperature behaviors of $\langle R^2(T)\rangle$ is controlled by the fraction $\phi(T)$, one can define in an operative way a transition temperature T_0 such that:

$$\phi(T_0) = 10^{-1} \Leftrightarrow T_0 = \frac{\Delta H}{\Delta S + k_B \ln(9)},$$

i.e.,

$$\frac{1}{T_0} = \frac{1}{T_m} + \frac{k_B \ln(9)}{\Delta H}, \tag{14}$$

where T_m, defined by $\phi(T_m) = 0.5$, is the temperature at which the energy-entropy compensation occurs. As defined, T_0, smaller than T_m, is the temperature at which ~10% of the protein fluctuations are of large amplitude, allowing particles to cross the free energy barrier of height $\Delta G = \ln(9)k_B T_0 \simeq 2k_B T_0$ at $T = T_0$. The transition temperature is independent of the observation time, but it depends upon both the energy gap and the entropy difference between conformational cages. We note, however, that in most experiments dealing with the dynamical transition the highest temperature investigated is always lower than T_m. The study of the higher temperature regime, $T > T_m$, requires taking into account additional processes like precursors to protein unfolding. It is worthwhile to note also that it is difficult to experimentally determine T_0 exactly because the transition is rather broad. However, Eq. 14 provides a simple relation between T_0 and other relevant parameters of the problem.

Now, to characterize the thermal mobility of a protein molecule within the temperature interval $\theta \le T < T_m$, we linearize Eq. 12b about a certain reference temperature T_r (e.g., $T_r = 300$ K) to obtain:

$$\langle R^2(T)\rangle \simeq \begin{cases} k_B T/k_1; & \theta < T < T_0, \\ k_B T/k_3 - a^2; & T_0 < T \sim T_m, \end{cases} \tag{15}$$

where

$$\frac{1}{k_3} = \frac{[1-\phi(T_r)]}{k_1}\left\{1 - \frac{\Delta H}{k_B T_r}\phi(T_r)\right\} + \frac{\phi(T_r)}{k_2}\left\{1 + \frac{\Delta H}{k_B T_r}[1-\phi(T_r)]\right\}, \tag{16a}$$

$$a^2 = \Delta H\left(\frac{1}{k_2} - \frac{1}{k_1}\right)\phi(T_r)[1-\phi(T_r)]. \tag{16b}$$

The force constant k_1 and the pseudo-force constant k_3 can thus be regarded as a measure of the degree of flexibility of

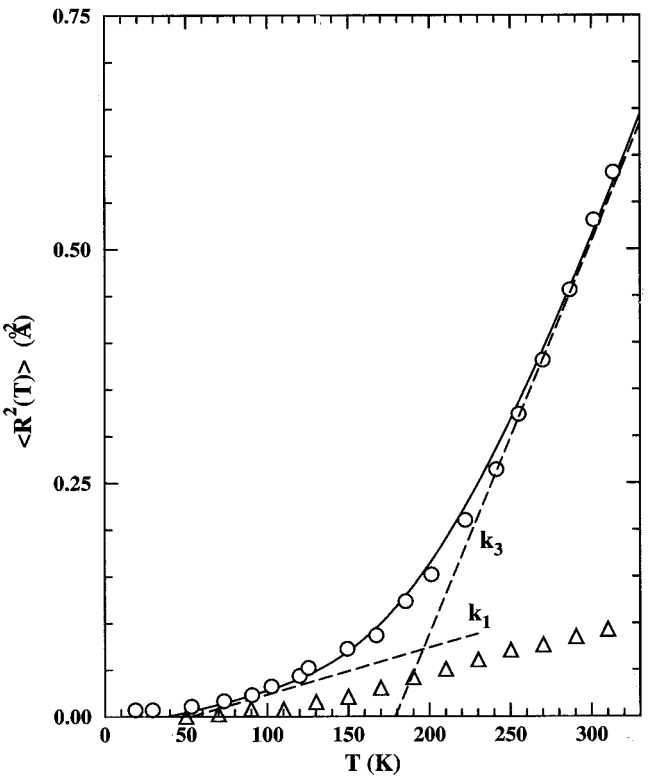

FIGURE 1 Hydrogen mean-square displacement $\langle R^2(T)\rangle = 3\langle x^2(T)\rangle$ versus temperature for hydrated myoglobin (*circles*) (from Doster et al., 1989). The solid line is the best fit to the data (*circles*) using the expression in Eq. 12b with parameters listed in Table 1. The quoted dashed curves correspond to linear approximations in Eq. 15 with the force constants k_1 and k_3 (see Table 1). The triangles represent elastic scans for the trehalose-coated CO-myoglobin (from Cordone et al., 1999). Note the absence of the dynamical transition for trehalose-coated CO-myoglobin.

a protein molecule, and as such they can be used to compare different systems having similar transition temperatures.

ILLUSTRATIVE APPLICATIONS AND DISCUSSION

As an illustration, we used the theory developed in the previous sections to analyze elastic temperature scans from the literature on myoglobin and purple membranes under different environmental conditions. Equation 12b, with $\phi(T)$ given in Eq. 8, and Eq. 14 constituted the main theoretical formulae to analyze experimental data. In both sets of experiments the data had been collected on backscattering spectrometers IN10, IN13, or IN16 at the ILL in Grenoble, with energy resolution ranging from 1 to 10 μeV, corresponding to a time window (or observation time) of $\sim\tau \simeq 1 - 0.1$ ns, and Q-range 0.6 − 4.5 Å^{-1} corresponding to fluctuations of ~1 Å.

Myoglobin has been widely used as a model protein for studies of dynamics (e.g., Frauenfelder et al., 1988) and the first neutron scattering experiments on the dynamical transition in a protein were on myoglobin powders hydrated with heavy water (D_2O) (Doster et al., 1989). Fig. 1 displays these experimental data (*circles*) and the best fit using Eq. 12b (*solid line*). The parameters extracted from the fit are listed in Table 1. We found that the transition temperature is $\sim T_0 \simeq 200$ K (compared to 180 K estimated by Doster et al.), the free energy barrier of the transition at 300 K is $\sim\Delta G \simeq 0.52$ kcal/mol, and the force constants associated to conformational fluctuations are $k_1 \simeq 2.76$ N/m in the harmonic regime at low temperature, and $k_2 \simeq 0.28$ N/m for larger fluctuations regime. The fit to low temperature ($T <$ 100 K) data using the leftmost expression in Eq. 10 gives a Debye temperature $\theta \simeq 110$ K corresponding to the low frequency $\omega_0 \simeq 38$ cm^{-1}. This is to say that Eq. 12b applies for temperatures $> \theta/2 \simeq 55$ K.

The dynamics of myoglobin in the presence of very high concentrations of the disaccharide, trehalose, has been studied by neutron scattering (Cordone et al., 1999). The elastic scan and density of state measurements showed that up to 320 K (the highest temperature examined) the system has a harmonic behavior. The authors suggested that the protective effect of trehalose on the biological structures is related to "trapping" them in a hard harmonic state even at high temperature. The fit to the data gave a Debye temperature $\theta \simeq 300$ K (i.e., $\omega_0 \simeq 210$ cm^{-1}) and a force constant of ~3.14 N/m. These data (*triangles*) are also reported in Fig. 1 where, as one can see, there is no discernible dynamical transition. The effect of the trehalose environment on the myoglobin dynamics would then be to increase both the Debye temperature and the dynamical transition temperature (by increasing ΔH and/or decreasing ΔS such that $T_0 >$ 320 K). The Doster et al. (1989) and Cordone et al. (1999) experiments emphasized the importance of the protein environment on its dynamics.

As another example we considered the purple membrane of *Halobacterium salinarum* that has been studied extensively by neutron scattering. It is made up of the retinal protein, bacteriorhodopsin, and specific lipids, and functions as a light-activated proton pump. By observing their respective dependence on hydration, correlations were established between dynamics and functional aspects such as photocycle kinetics and conformational changes (Zaccai, 2000b). Different populations of motions were also found in purple membranes, depending on energy resolution (time window) (Fitter et al., 1996), scattering vector range (space window) (Réat et al., 1997), H-D labeling of different parts of bacteriorhodopsin (Réat et al., 1998), or hydration dependence (Lehnert et al., 1998). We note that within the framework of our analysis, the expression different populations of motions means that there are fractions of particles that are dynamically nonequivalent, i.e., $x_\alpha \neq 1$. The motions for each dynamical category α of particles was fitted in terms of the model with a small and a large conformational cage as outlined above.

Fig. 2 *A* shows results from the dry sample, and Fig. 2, *B* and *C* from the wet ones, Fig. 2 *B* describing only the

TABLE 1 Summary of parameters obtained from the best fits to data in Figs. 1 and 2

Parameters	Myoglobin (hydrated)	PM dry (unlabeled)	PM wet (labeled core)	Native PM wet		
				$x_1 = 0.57$	$x_2 = 0.43$	Average
ΔH (kcal/mol)	1.59	1.08	1.57	1.57	9.53	5
ΔS (R)	1.80	1.30	1.65	1.65	14	7
ΔG_0 (kcal/mol)	0.88	0.70	0.90	0.90	1.30	1.07
ΔG (kcal/mol)	0.52	0.30	0.59	0.59	1.18	0.84
T_m (K)	444	420	480	480	340	358
T_0 (K)	200	156	205	205	293	272
k_1 (N/m)	2.76	1.56	2.24	2.24	1.06	1.51
k_2 (N/m)	0.28	0.38	0.23	0.23	0.028	0.06
k_3 (N/m)	0.33	0.44	0.28	0.28	0.014	0.03

ΔH and ΔS are the energy and entropy differences for the system in the large and small conformational cages, respectively. $\Delta G_0 = \ln(9)\, RT_0$ and ΔG represents the free energy barrier of the transition at T_0 and 300 K, respectively ($RT \simeq 0.6$ kcal/mol at 300 K). The energy-entropy compensation temperature is $T_m = \Delta H/\Delta S$, and the transition temperature T_0 is calculated from Eq. 14. k_1 and k_2 are the force constants associated to the small and large conformational cage, respectively (see Eq. 12b), and k_3 is the force constant at 300 K. x_1 and x_2 denote the population fraction.

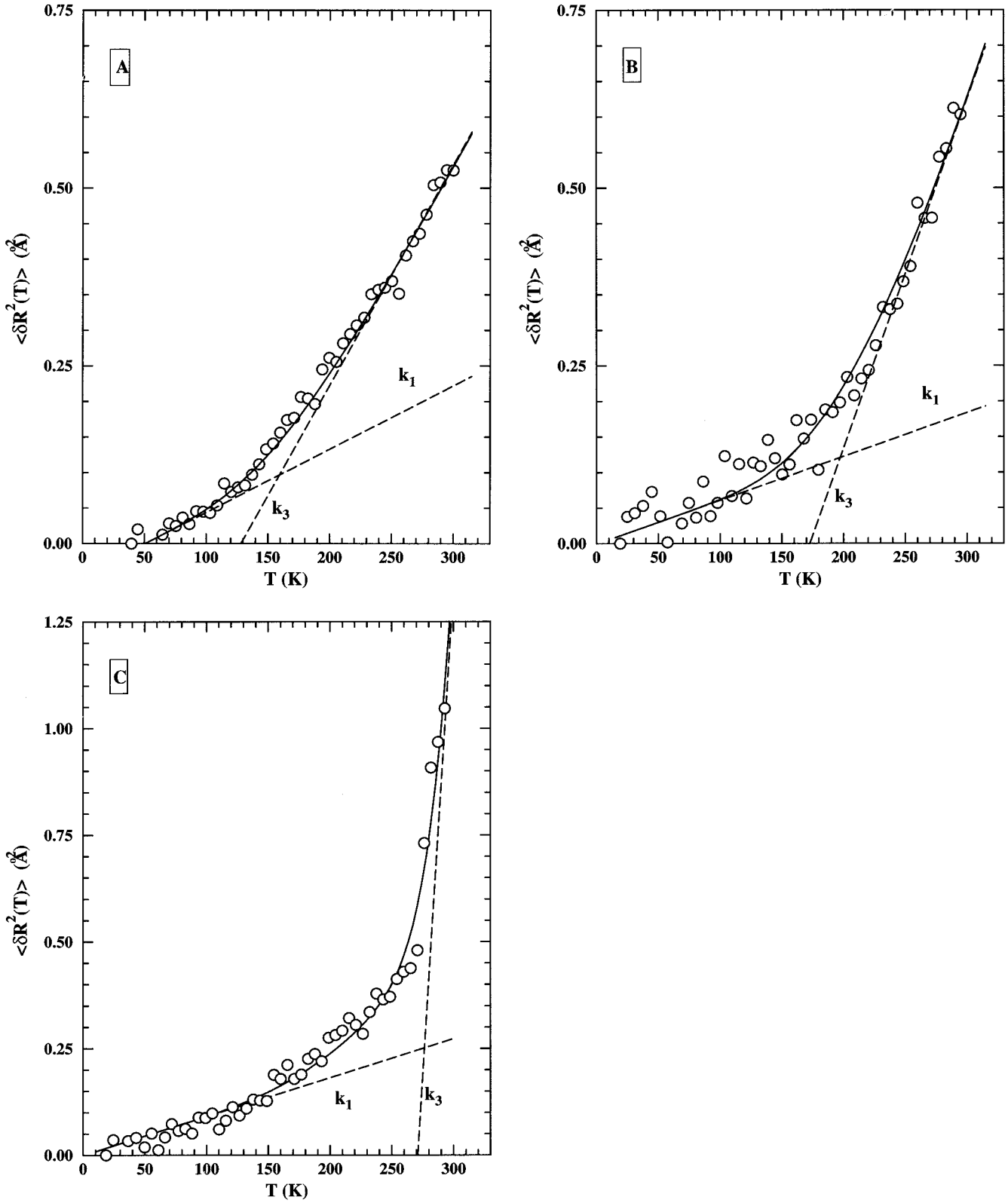

FIGURE 2 Hydrogen mean-square displacement $\langle \delta R^2(T) \rangle = \langle R^2(T) \rangle - \langle R^2(T_{\min}) \rangle$ (with $2\langle R^2 \rangle = \langle u^2 \rangle$) versus temperature for the purple membrane (PM) bacteriorhodopsin (from Réat et al., 1998). The solid lines are best fits to the data (*circles*) using the expression in Eq. 12b with parameters listed in Table 1. The quoted dashed curves correspond to linear approximations in Eq. 15 with force constants k_1 and k_3 (see Table 1). Panel *A* refers to unlabeled PM dry, *B* to labeled core PM wet, and *C* to native PM wet. For panel *C* the solid line through the data is obtained using Eq. 13 for two populations $\langle \delta R^2(T) \rangle = \Sigma_{\alpha=1}^{2} x_\alpha \langle \delta R_\alpha^2(T) \rangle$, where $\langle \delta R_1^2(T) \rangle$ corresponds to *B*.

protein core (data from a sample with labeled amino acids and retinal). The data in Fig. 2, *A* and *B* were fitted by using Eq. 12b (*solid line*) for a single population model, while data in Fig. 2 *C* required using a two-population model (i.e., Eq. 13) for a better fit (*solid line*) over the entire range of temperature (see Table 1 for parameters). In this latter case (i.e., Fig. 2 *C*), we found that 57% of the total mean-square displacements are represented by motions of the protein core identical to that in Fig. 2 *B*.

Comparison of parameters in Table 1 corresponding to Fig. 2, *A* and *C* shows that the underlying dynamics of the dry sample is very different from that of the wet one (i.e., single population versus two populations) underlining again the importance of the protein environment on the dynamics. In addition, a similar comparison between data in Fig. 2, *A* and *B* (both being fitted with a single population, i.e., $x_\alpha = 1$) indicated that the bacteriorhodopsin core (even when wet) is less flexible than the dry sample as a whole because the transition temperature, the free energy barrier of the transition, and the force constants of the protein core are all higher than those of the dry sample.

The data in Fig. 2 *C*, from Lehnert et al. (1998), were obtained for *Q*-range ($0.3\ \text{Å}^{-1} < Q < 1.8\ \text{Å}^{-1}$). These authors also analyzed what they named a "small amplitude" population of membrane motions in a higher *Q*-range ($2.4\ \text{Å}^{-1} < Q < 3.6\ \text{Å}^{-1}$). The Gaussian approximation is still valid since $Q^2\langle R^2\rangle \leq 1$ for these motions. We performed our model fit to these data (not shown) to examine whether this high *Q* population corresponds to one of the two found in the low *Q* data. The total high *Q* mean-square displacements are described by a single population with the parameters $\Delta H = 1.78$ kcal/mol, $\Delta S = 1.14$ R, $k_1 = 1.88$ N/m, $k_2 = 0.48$ N/m, and $T_0 = 267$ K. A comparison with values in Table 1 shows that the thermodynamic parameters are similar to those of population 1 in the low *Q* analysis, except for T_0, which is close to the average value for the two populations.

In order to speculate on the two-population interpretation of the wet sample, we recall that 60% of amino acid residues of bacteriorhodopsin are in the seven transmembrane helices, and 40% are in solvent-exposed loops linking the helices and N and C-terminal. Thus, a conceivable assignment is that the first population is formed by the alpha helices (constrained) in the membrane and the second one by the remaining solvent-exposed parts of the protein that can experience larger fluctuations within larger conformational cages (see ΔS values in Table 1). This is consistent and provides support for finding that 57% and 43% of contributions to the total mean-square displacements in Fig. 2 *C* come from populations 1 and 2, respectively. In addition, the free energy barrier ΔG is of order of RT for population 1, while it is about twice as large for population 2. According to these considerations, population 1 ($x_1 = 0.57$) would describe the dynamics of the protein core and population 2 ($x_2 = 0.43$) the dynamics of loops in solvent for which the associated $\Delta H \simeq 9.53$ kcal/mol corresponds to that of one to two H-bonds (H-bond energy lies between 3 and 6 kcal/mol). As expected, comparison of force constants indicates that population 2 is more flexible than population 1. At physiological temperature (i.e., above the solvent melting point at 270 K) the active core of the wet protein is about a factor of 10 more resilient than the wet membrane as a whole.

Finally, we compared the dynamics of the hydrated myoglobin and hydrated purple membrane in Fig. 3 through the curves obtained from best fits to experimental data in Figs. 1 and 2. It appears that the transition temperature, the free energy barrier of the transition, and force constants are very similar for myoglobin and the bacteriorhodopsin core. At low temperatures the highest force constant is for myoglobin, followed by the bacteriorhodopsin core, then purple membranes (see Table 1). At the higher temperatures the myoglobin and bacteriorhodopsin core have similar behavior as a function of *T* and thus show similar force constant values (see Table 1), consistent with the compact structure of the alpha-helical myoglobin, which does not have any large surface loops. However, because of the two populations in the wet membrane (with different transition temperatures) the elastic scans for the purple membrane and for the bacteriorhodopsin core diverge at ~260 K, with the

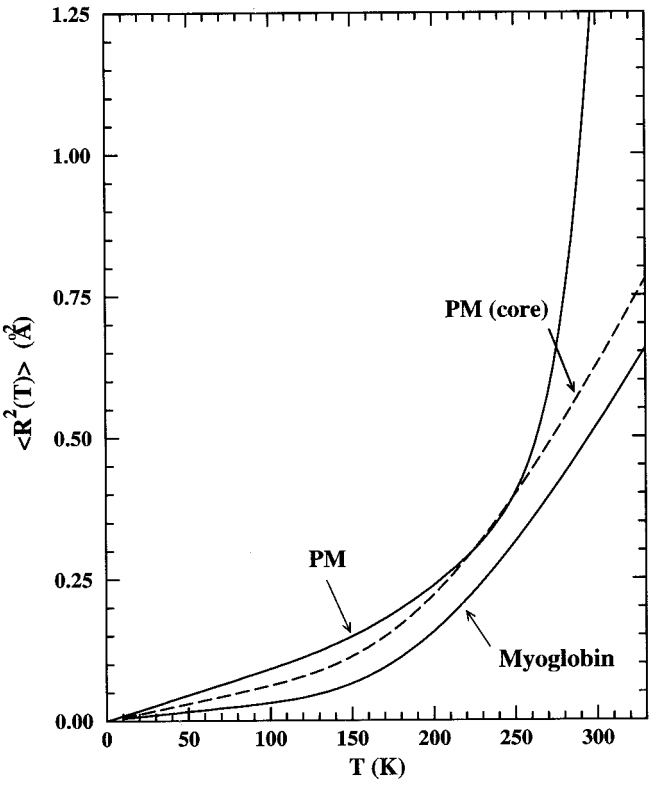

FIGURE 3 Comparison between hydrated myoglobin in Fig. 1 and native PM wet and labeled core PM wet (*dashed line*) in Fig. 2, *B* and *C*, respectively.

membrane scan displaying a very low (10 times smaller) force constant value, 0.03 N/m, at physiological temperature.

To conclude, the time window examined in the above elastic scans corresponds mainly to H atoms moving with the amino acid side chains of the protein (Smith, 1991). Thus, it may be instructive to analyze values in Table 1 with this perspective. The number of nonexchangeable H atoms in side chains varies from 1 (for glycine) to 9 (for leucine and iso-leucine), with a mean value of 5 H per amino acid, calculated for the composition of myoglobin, for example. The H-bond energy is $\Delta H_H \simeq 3-6$ kcal/mol; the stretching k_H^S and bending k_H^B force constants associated to an H bond are ~13 N/m and 2–3 N/m (Chou, 1985; Itoh and Shimanouchi, 1970), respectively, while the force constant for a typical covalent bond falls in the range of 100–400 N/m. It results from the above analysis that the dynamical transition is associated with typical free energy barriers of the order of the thermal energy, RT, and typical force constants ranging from 0.1 to 3 N/m, similar to k_H^B. Moreover, except for the purple membrane at 270 K, the energies for the dynamical transition correspond to ~1 H bond per amino acid side chain since $5\Delta H \sim \Delta H_H$. As already noticed by Doster and Settles (1999), these observations tend to suggest that the H-bond networks within the protein and between protein and solvent play a key role in the dynamical transition.

Thanks are due to C. Pfister and the IN13 group for stimulating discussions and comments on the manuscript, and to P. Nozières and the theory group of ILL for their hospitality.

REFERENCES

Andreani, C., A. Filabozzi, F. Menzinger, A. Desideri, A. Deriu, and D. Di Cola. 1995. Dynamics of hydrogen atoms in superoxide dismutase by quasielastic neutron scattering. *Biophys. J.* 68:2519–2523.

Bée, M. 1988. Quasielastic Neutron Scattering. Adam Hilger, Bristol.

Brooks, C. L. III, M. Karplus, and B. M. Pettitt. 1988. Proteins: a theoretical perspective of dynamics, structure, and thermodynamics. *In* Advances in Chemical Physics, Vol. LXXI. I. Prigogine and S. A. Rice, editors. John Wiley & Sons, New York. 74–95.

Chou, K.-C. 1985. Low-frequency motions in protein molecules. *Biophys. J.* 48:289–297.

Cordone, L., M. Ferrand, E. Vitrano, and G. Zaccai. 1999. Harmonic behavior of trehalose-coated carbon-monoxy-myoglobin at high temperature. *Biophys. J.* 76:1043–1047.

Creighton, T. E. 1991. Stability of folded conformations. *Curr. Opin. Struct. Biol.* 1:5–16.

Doster, W., S. Cusack, and W. Petry. 1989. Dynamical transition of myoglobin revealed by inelastic neutron scattering. *Nature.* 337: 754–756.

Doster, W. S., and M. Settles. 1999. The dynamical transition in proteins: the role of hydrogen bonds. *In* Hydration Processes in Biology: Theoretical and Experimental Approaches, Nato Science Series A: Life Science, Vol. 305. M.-C. Bellissent-Funel, editor. IOS Press, Berlin. 177–191.

Ferrand, M., A. J. Dianoux, W. Petry, and G. Zaccai. 1993. Thermal motions and function of bacteriorhodopsin in purple membranes: effects of temperature and hydration studied by neutron scattering. *Proc. Natl. Acad. Sci. USA.* 90:9668–9672.

Fitter, J., R. E. Lechner, N. A. Dencher, and G. Büldt. 1996. Internal molecular motions of bacteriorhodopsin: hydration-induced flexibility studied by quasielastic incoherent neutron scattering using oriented purple membranes. *Proc. Natl. Acad. Sci. USA.* 93:7600–7605.

Frauenfelder, H., F. Parak, and R. D. Young. 1988. Conformational substates in proteins. *Annu. Rev. Biophys. Biophys. Chem.* 17:569–572.

Götze, W., and L. Sjögren. 1992. Relaxation processes in supercooled liquids. *Rep. Prog. Phys.* 55:241–376.

Itoh, K., and T. Shimanouchi. 1970. Vibrational frequencies and modes of α-helix. *Biopolymers.* 9:383–399.

Kneller, G. R., and J. C. Smith. 1994. Liquid-like side-chain dynamics in myoglobin. *J. Mol. Biol.* 242:181–185.

Lehnert, U., V. Réat, M. Weik, G. Zaccai, and C. Pfister. 1998. Thermal motion in bacteriorhodopsin at different hydration levels studied by neutron scattering: correlation with kinetics and light-induced conformational changes. *Biophys. J.* 75:1945–1952.

Loncharich, R. J., and B. R. Brooks. 1990. Temperature dependence of dynamics of hydrated myoglobin: comparison of force-field calculations and neutron scattering data. *J. Mol. Biol.* 215:439–455.

Parak, F., E. W. Knapp, and D. Kucheida. 1982. Protein dynamics. Mössbauer spectroscopy on deoxymyoglobin crystals. *J. Mol. Biol.* 161: 177–194.

Rasmussen, B. F., A. M. Stock, D. Ringe, and A. G. Petsko. 1992. Crystalline ribonuclease A loses function below the dynamical transition at 220 K. *Nature.* 357:423–424.

Réat, V., R. Dunn, M. Ferrand, J. L. Finney, R. M. Daniel, and J. C. Smith. 2000. Solvent dependence of dynamic transitions in protein solutions. *Proc. Natl. Acad. Sci. USA.* 97:9961–9966.

Réat, V., H. Patzelt, M. Ferrand, C. Pfister, D. Oesterhelt, and G. Zaccai. 1998. Dynamics of different functional parts of bacteriorhodopsin: H-^{2}H labeling and neutron scattering. *Proc. Natl. Acad. Sci. USA.* 95: 4970–4975.

Réat, V., G. Zaccai, M. Ferrand, and C. Pfister. 1997. *In* Biological Macromolecular Dynamics. S. Cusack, H. Büttner, M. Ferrand, P. Langan, and P. Timmins, editors. Adenine Press, New York. 117–122.

Smith, J. C. 1991. Protein dynamics: comparison of simulations with inelastic neutron scattering. *Q. Rev. Biophys.* 24:227–291.

Smith, J., K. Kuczera, and M. Karplus. 1990. Dynamics of myoglobin: comparison of simulation results with neutron scattering spectra. *Proc. Natl. Acad. Sci. USA.* 87:1601–1605.

Zaccai, G. 2000a. How soft is a protein? A force constant approach to protein dynamics measured by neutron scattering. *Science.* 288: 1604–1607.

Zaccai, G. 2000b. Moist and soft, dry and stiff: a review of neutron experiments on hydration-dynamics-activity relations in the purple membrane of *Halobacterium salinarum. Biophys. Chem.* 86:249–257.